J. Electrochem. Sci. Eng. **16** (2026) 3227; https://doi.org/10.5599/jese.3227

Open Access : : ISSN 1847-9286
https://pub.iapchem.org/ojs/index.php/JESE

Original scientific paper

Carbon nitride-assisted thermal treatment for sintering-resistant Pt/C catalysts

Junyi Li[1], Liang Tian[2,✉] and Ying Wang[3,✉]

[1]*School of Materials Science and Engineering, Peking University, Beijing 100871, China*
[2]*Instituto de Tecnología Química, Consejo Superior de Investigaciones Científicas-Universitat Politècnica de Valencia, Universitat Politècnica de Valencia, Av. De los Naranjos s/n, 46022 Valencia, Spain*
[3]*State Key Laboratory of Green Papermaking and Resource Recycling, Qilu University of Technology (Shandong Academy of Sciences), Jinan 250353, China*

Corresponding Authors: ✉ltian@itq.upv.es; ✉wangying93@qlu.edu.cn

Received: January 10, 2026; Accepted: March 5, 2026; Published: March 9, 2026

Abstract

High-temperature annealing often induces severe sintering of Pt nanoparticles in Pt/C catalysts, resulting in activity degradation. Here, a carbon nitride–assisted thermal treatment strategy is proposed to enhance the thermal stability of Pt/C. TG-FTIR and XPS analysis reveal that nitrogen-containing species generated during carbon nitride decomposition play a key role in suppressing Pt nanoparticle coalescence at intermediate temperatures. Although the carbon nitride framework decomposes at high temperatures, residual graphitic and pyridinic nitrogen species are retained and interact electronically with Pt, leading to a reduced Pt binding energy. As a result, the carbon nitride–assisted Pt/C maintains a narrow particle size distribution after annealing. Electrochemical measurements demonstrate that the assisted catalyst retains oxygen reduction reaction activity comparable to commercial Pt/C after thermal treatment at 700 °C, while the untreated sample shows pronounced performance loss. Moreover, the assisted catalyst exhibits significantly improved durability after 20 000 cycles. This work offers a simple and effective approach to improving the thermal robustness of Pt-based electrocatalysts for PEM fuel cells.

Keywords

Carbon nitride decomposition; platinum nanoparticles; sintering suppression; oxygen reduction reaction; electrochemical durability

Introduction

Proton exchange membrane fuel cells (PEMFCs) represent a promising energy conversion technology toward carbon-neutral energy systems. However, the slow kinetics of the cathodic

oxygen reduction reaction (ORR) and the high cost of catalysts remain key bottlenecks to its large-scale application. Currently, platinum-based carbon-supported catalysts (Pt/C) dominate due to their excellent activity and mature processes [1-3]. However, the scarcity of platinum resources and high prices have prompted researchers to adopt strategies such as improving platinum atom utilization and enhancing catalyst stability to alleviate platinum dosage and durability issues.

Current efforts to improve the ORR performance of Pt/C catalysts primarily focus on alloying, support engineering, and structural optimization, often relying on high-temperature thermal treatment [4-10].

However, such treatments inevitably induce Pt nanoparticle coarsening *via* Ostwald ripening, leading to severe loss of electrochemically active surface area (ECSA) and creating a trade-off between process optimization and catalytic performance. Therefore, developing strategies to suppress Pt sintering during high-temperature treatment is crucial for advancing Pt/C catalyst performance.

As is well known, surface ligands are a common method to improve the stability of metal nanoparticles, but the interaction between ligands and carbon supports is weak and they decompose and fail at high temperatures. Recently, the process of reducing catalyst deactivation by coating the catalyst surface has received widespread attention, particularly the inert atomic-layer coating of metal catalysts, which has been reported to significantly improve their catalytic activity and stability [11,12]. However, synthesizing atomic layer coatings is very challenging, and an excessively thick shell structure will hinder mass transfer, leading to a significant decrease in activity. Therefore, the development of a dynamic confined system that combines high-temperature stability and interfacial reactivity has become a challenging problem in the field. Previous studies have shown that nitrogen doping/modification (via methods such as heteroatom-doped carbon synthesis, surface functionalization, or post-treatment) of carbon supports can improve the performance and durability of Pt/C electrocatalysts by enhancing Pt dispersion and strengthening metal-support interactions [13-16]. However, many reported strategies rely on pre-synthesized N-doped carbon supports, which usually require additional synthesis steps and are often tailored to specific catalyst systems.

Carbon nitride polymer materials exhibit excellent support functions in the field of photo (/electro)-catalysis due to their nitrogen-rich electronic structure and tuneable interfacial chemistry. Their triazine ring skeleton and abundant functional groups such as amino ($-NH_2$), imine (-NH-) and cyano (-C≡N) on the surface can form strong interactions with metal species (such as nanoparticles, single atoms, *etc*.) through coordination or electrostatic adsorption, giving them excellent metal anchoring ability [17-22]. However, existing research on carbon nitride is mostly focused on photocatalytic systems [23-27], and its mechanism for auxiliary regulation of metal anchoring in catalyst synthesis remains unclear. Based on the unique advantages of carbon nitride materials and the balance between traditional static confinement strategies (such as carbon coating and core-shell structures) in improving the high-temperature stability and activity of metal nanoparticles, this study proposed an auxiliary heat treatment strategy for polymer carbon nitride (g-C_3N_4). By constructing a synergistic mechanism of "thermodynamic anchoring (N-Pt bonding)" and "kinetic hindrance (nitrogen defect steric confinement)", the migration behaviour of Pt nanoparticles under high-temperature conditions is effectively suppressed.

Experimental

Preparation of samples

Commercial Pt/C (20 wt.% Pt on Vulcan XC-72, donated as Pt/C) was purchased from Shanghai Macklin Biochemical Industrial Co., Ltd. g-C_3N_4 was prepared by using the conventional method

reported previously [28,29]. In this case, typically 10 g of melamine was placed in an alumina crucible with a lid and heated at 4 °C min^{-1} to 550 °C, then held at 550 °C for 5 h. The resultant yellow material was milled to a fine powder using a mortar and pestle. Carbon nitride–assisted Pt/C catalysts were synthesized at 400, 500, 600, 700, 800 and 900 °C (denoted as 400GPtC, 500GPtC, 600GPtC, 700GPtC, 800GPtC and 900GPtC, respectively). In a typical process, commercial Pt/C (25 mg) and g-C_3N_4 (2.5 mg) were separately dispersed in acetone (1 mL) and ultrasonicated to obtain homogeneous suspensions. The two suspensions were then combined and magnetically stirred until complete solvent evaporation. The resulting solid was further dried in an oven at 60 °C for 5 h. Subsequently, the dried powder was subjected to thermal treatment under an argon atmosphere, with a heating rate of 4 °C min^{-1} up to 700 °C, followed by holding at this temperature for 3 h. After naturally cooling to room temperature, the g-C_3N_4–assisted Pt/C catalyst was obtained.

For comparison, commercial Pt/C also undergoes the same heat treatment at different temperatures (denoted as 400PtC, 500PtC, 600PtC, 700PtC, 800PtC and 900PtC, respectively).

Sample characterization

Phases in the samples were identified using an X-ray diffractometer (XRD, X'Pert Pro, Philips, Netherlands) with Cu-Kα radiation (λ = 15.406 nm) operated at 40 kV and 40 mA, at a scanning rate of 2° min^{-1} and a step size of 2θ = 0.02°. X-ray photoelectron spectroscopy (XPS) examination was carried out on a VG Multilab 2000 instrument (Thermo Electron Co., USA) using 300 W Al Kα as the excitation source. In this case, the samples were subjected to high vacuum before being introduced into the analysis chamber. The binding energies from XPS were referenced to the C1s binding energy (284.6 eV) of "adventitious" carbon contamination. Morphologies of product phases were examined using a transmission electron microscope (TEM, 2000F, Jeol Ltd., Japan) (TEM samples were loaded onto a copper microgrid coated with a thin amorphous carbon film). Fourier transform infrared (FTIR) spectra of samples (embedded in KBr pellet) were recorded within the frequency range of 4000 to 500 cm^{-1} and with a resolution of 4 cm^{-1} using a FTIR spectrometer (VERTEX 70, Germany). Thermogravimetric (TG) analysis was performed by a thermogravimetric analyser (TA Instruments, Q5000IR). TG-FTIR measurements were performed using a Bruker FTIR spectrometer coupled with a NETZSCH STA 449 F5 thermal analyser (Bruker TGA-IR / NETZSCH STA 449 F5).

Electrochemical measurements

Electrochemical measurements were performed on a CHI760e electrochemical workstation (Chenhua Instruments, Shanghai, China). The electrocatalytic performances of the catalysts were evaluated using a rotating disk electrode (RDE). The RDE was employed as a working electrode (5 mm in diameter), a Pt plate (10×10 mm, 0.1 mm thick) was used as the counter electrode, and the Ag/AgCl (saturated KCl, with a salt bridge) was utilized as the reference electrode. All potentials were experimentally converted to values referenced to the reversible hydrogen electrode (RHE). The reference electrode was calibrated to RHE in H_2-saturated 0.1 M $HClO_4$.

The as-prepared catalysts were dispersed in a mixture containing ethanol and Nafion (5 vol.%, 1.9 : 0.1 mL) to form a 5 mg condition and 4 μL of the ink was cast on the glassy carbon and dried under ambient conditions. The Pt mass loading was calculated to be: Pt mass per disk: 2.0 μg; Pt mass loading: 10.2 μg cm^{-2}.

The cyclic voltammetry (CV) measurements were performed in N_2-saturated 0.1 M $HClO_4$ solutions at a scan rate of 50 mV s^{-1} after catalyst activation. The electrochemically active surface area (ECSA) was calculated by integrating the hydrogen underpotential deposition (H_{upd}) peak in cyclic voltammetry. The oxygen reduction reaction (ORR) polarization curves were recorded in

O_2-saturated 0.1 M $HClO_4$ using a rotating-disk electrode at a rotation rate of 1,600 rpm and a sweep rate of 10 mV s^{-1}. ORR activity was evaluated by comparing the LSV polarization curves and the corresponding half-wave potentials, because mass activity is not suitable for a meaningful comparison across all samples in this study: for severely deactivated catalysts, the current at 0.90 V is extremely low (or negligible), making mass-activity values at this potential unreliable and not representative of their overall ORR behaviour.

Accelerated durability test (ADT) was performed at room temperature by applying cyclic sweeps between 0.6 and 1.0 V *vs*. RHE in O_2-saturated 0.1 M $HClO_4$ at a sweep rate of 100 mV s^{-1}. All polarization curves were *iR* corrected.

Results and discussion

The morphology and particle-size evolution of Pt nanoparticles were compared by TEM for the commercial Pt/C catalyst, the commercial Pt/C after heat treatment at 500 °C, and the commercial Pt/C modified with g-C_3N_4, followed by the same thermal treatment. As shown in the TEM images and the corresponding particle size distribution histograms (Figure 1), the as-received commercial Pt/C exhibits well-dispersed Pt nanoparticles with an average particle size of approximately 2.4 nm and a relatively narrow size distribution. After thermal treatment at 500 °C, pronounced particle coarsening is observed for the commercial Pt/C, characterized by a significant increase in the average particle size to 3.5 nm and a broadened size distribution, indicative of severe nanoparticle sintering. In contrast, the g-C_3N_4-modified commercial Pt/C subjected to 500 °C annealing retains much smaller Pt nanoparticles with an average size of around 2.6 nm, along with a notably narrower particle size distribution.

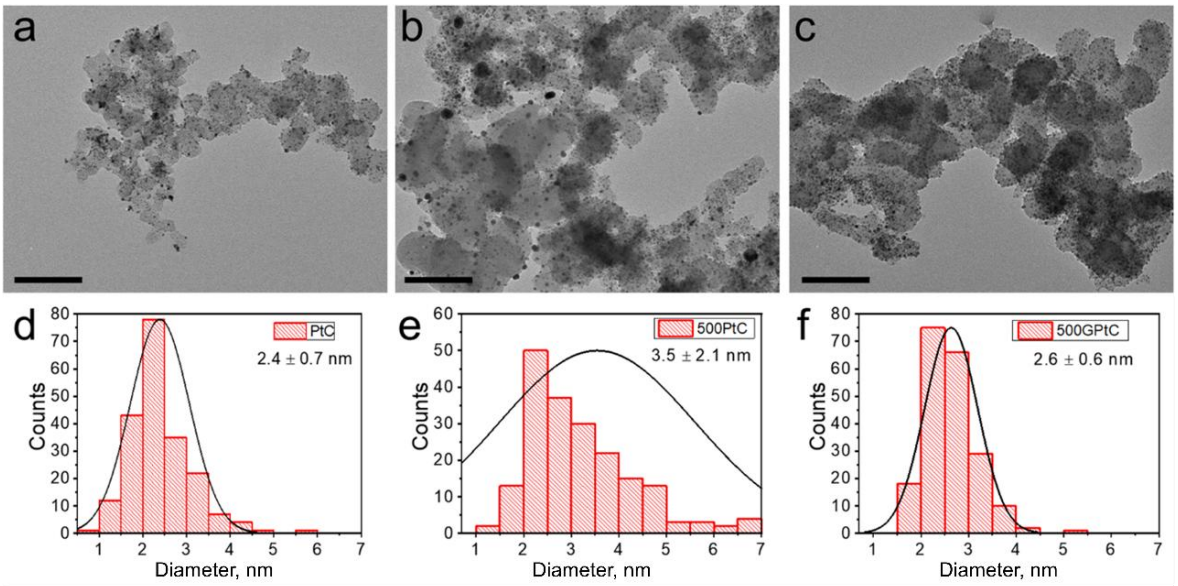

Figure 1. *TEM images and corresponding particle size distribution histograms of different samples: (a) and (d) commercial Pt/C, (b) and (e) commercial Pt/C heat-treated at 500 °C, (c) and (f) Pt/C with added g-C_3N_4 heat-treated at 500 °C. All scale bars are 100 nm*

The difference in carbon support in Pt/C (Vulcan XC-72) may be from an intrinsic particle/aggregate size distribution or some variation during the treatment process. These results clearly demonstrate that the introduction of g-C_3N_4 effectively suppresses the thermally induced sintering of Pt nanoparticles during heat treatment.

The thermal sintering behaviour of Pt/C was further investigated by TEM analysis after heat treatment at different temperatures (500, 600, 700, 800 and 900 °C). As shown in the TEM images and the corresponding particle size distribution histograms (Figure 2), a pronounced increase in the

average Pt nanoparticle size was observed with increasing annealing temperature, accompanied by a progressively broadened size distribution. This size evolution is consistent with a thermally driven ripening process, such as Ostwald ripening, in which smaller Pt nanoparticles gradually dissolve and redeposit onto larger ones during high-temperature treatment, leading to the growth of larger particles at the expense of smaller ones.

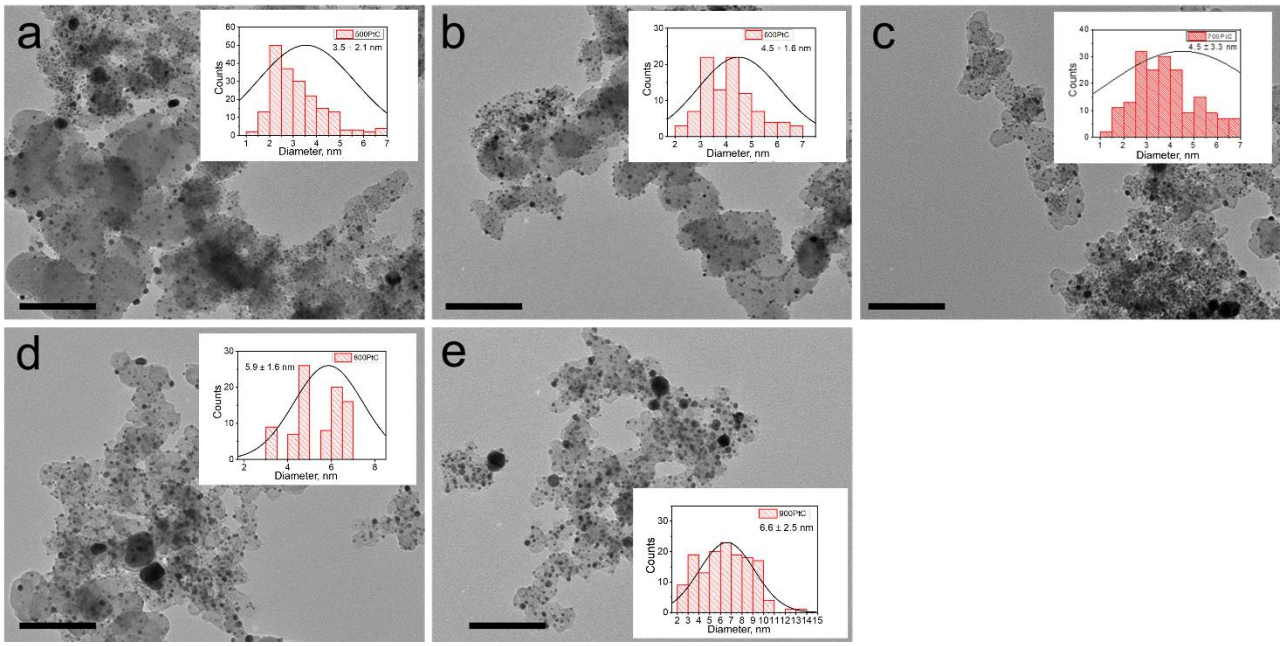

Figure 2. *TEM images and corresponding particle size distribution histograms of commercial Pt/C heat-treated at (a) 500; (b) 600; (c) 700; (d) 800 and (e) 900 °C. All scale bars are 100 nm*

The effect of carbon nitride addition on the thermal sintering behaviour of Pt/C was also examined by TEM after heat treatment at various temperatures (Figure 3). In contrast to pristine Pt/C, the Pt nanoparticles in the carbon nitride-modified Pt/C exhibited remarkable resistance to particle growth upon thermal annealing.

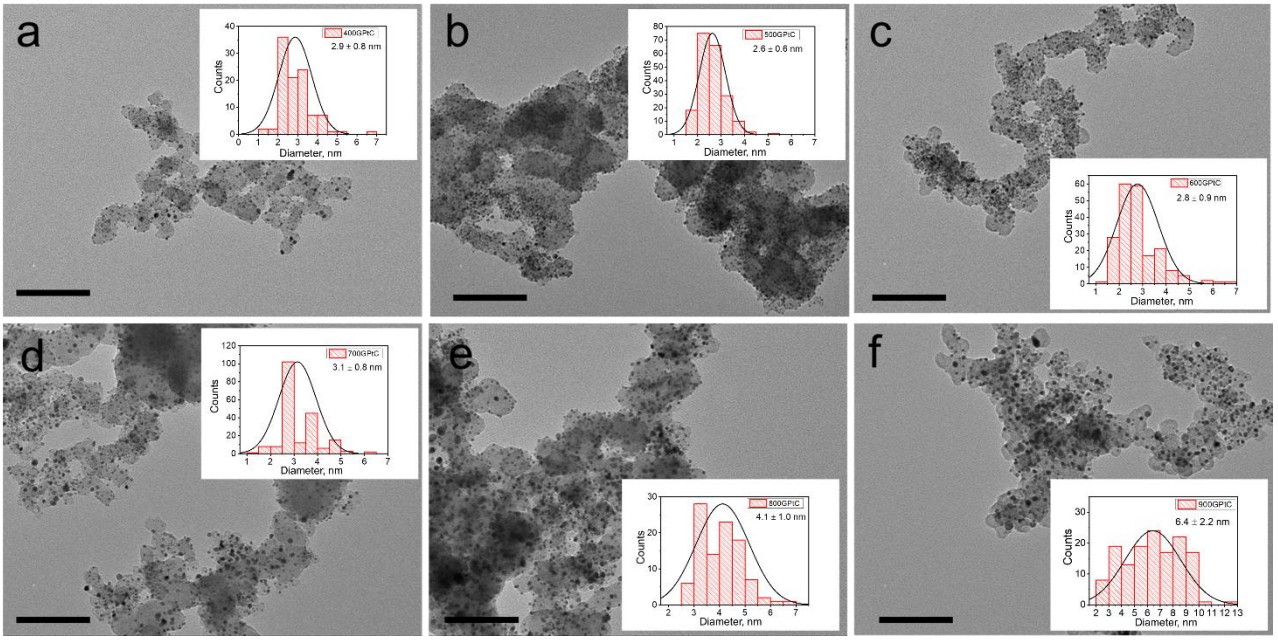

Figure 3. *TEM images and corresponding particle size distribution histograms of Pt/C with added g-C_3N_4 heat-treated at (a) 400; (b) 500; (c) 600; (d) 700; (e) 800 and (f) 900 °C. All scale bars are 100 nm*

As revealed by TEM images and corresponding particle size distribution histograms, the average Pt particle size increased only slightly up to 700 °C, remaining 2.6 to 3.1 nm, indicating effective suppression of high-temperature Ostwald ripening. Moreover, the particle size distribution became noticeably narrower compared to that of Pt/C without carbon nitride, suggesting improved uniformity of Pt nanoparticles after thermal treatment.

The phase evolution and thermal sintering behaviour of Pt nanoparticles were further investigated by X-ray diffraction (XRD) using g-C_3N_4-assisted Pt/C (denoted as GPtC) subjected to heat treatment at temperatures ranging from 400 to 900 °C, with pristine Pt/C serving as a reference. As shown in Figures 4a and 4b, the XRD patterns of both samples exhibit characteristic diffraction peaks corresponding to metallic Pt, with noticeable differences in peak intensity and broadening as a function of annealing temperature.

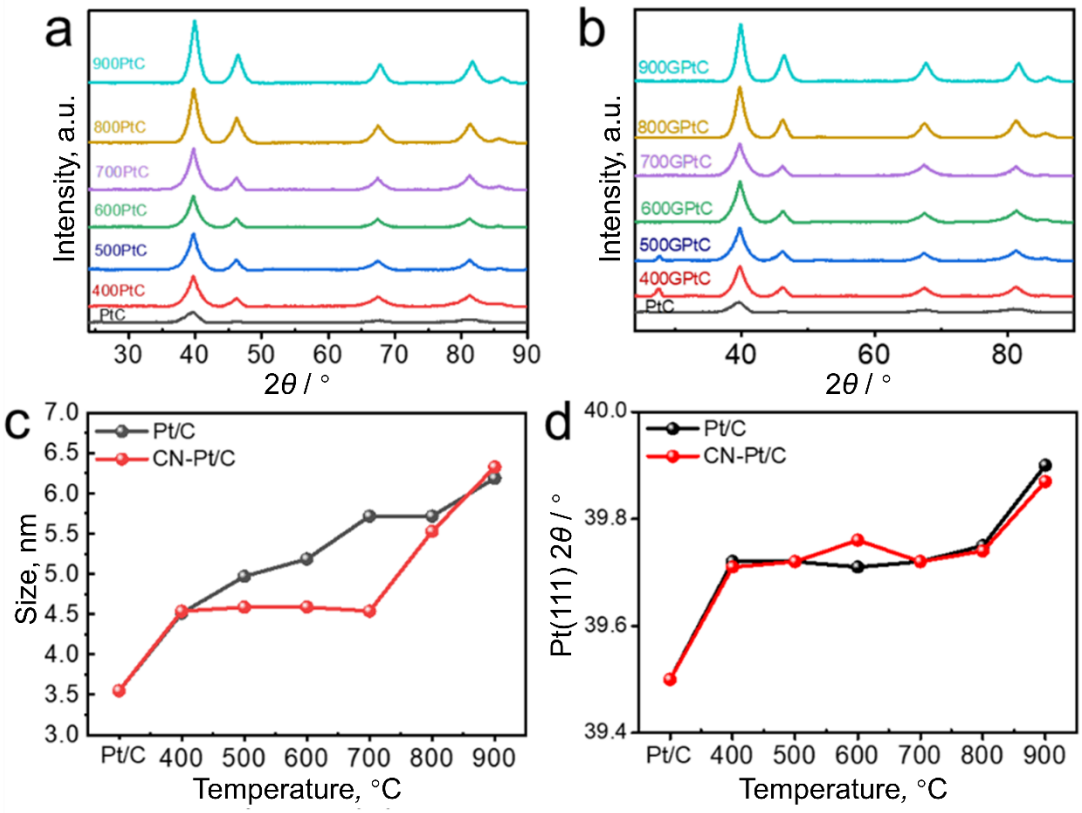

Figure 4. *XRD patterns of (a) Pt/C and (b) g-C_3N_4 assisted Pt/C at different heat treatment temperatures; (c) Pt grain size and (d) Pt (111) crystal plane diffraction peak position as a function of heat treatment temperature*

The Pt crystallite sizes calculated using the Scherrer equation are summarized in Figure 4c. It is evident that the introduction of g-C_3N_4 significantly suppresses the growth of Pt crystallites within the temperature range of 500 to 700 °C, resulting in smaller crystallite sizes compared to Pt/C treated at the same temperatures. In addition, the temperature-dependent evolution of the Pt (111) diffraction peak position is shown in Figure 4d, indicating that the Pt lattice parameter is predominantly governed by the thermal treatment temperature and shows negligible dependence on the presence of g-C_3N_4.

To elucidate the role of carbon nitride during the thermal treatment process, the thermal decomposition behaviour of g-C_3N_4 was first investigated by combined TG-FTIR and TG-DTA analyses. As revealed by the TG-FTIR results (Figure 5a), the evolution of gaseous species associated with carbon nitride decomposition becomes detectable at approximately 500 °C, where the

emergence of cyano-containing species is observed. Upon further increasing the temperature to around 600 °C, g-C_3N_4 undergoes pronounced decomposition, accompanied by the release of cyano, amino, and triazine-related fragments. Consistently, the TG-DTA profile (Figure 5b) shows the onset of mass loss at about 500 °C, followed by an accelerated decomposition process above 600°C, and the complete decomposition of g-C_3N_4 at approximately 750 °C. In this TG-DTA measurement, the DTA trace records the differential thermal response of the sample relative to an inert reference under the same heating program; the ordinate is defined as the mass-normalized thermal effect (mW mg^{-1}), an instrument-calibrated heat-flow-like signal, that is proportional to the temperature difference ($\Delta T = T_{sample} - T_{ref}$), with the peak direction (endothermic/exothermic) following the instrument's sign convention. Accordingly, an accelerated decomposition process is observed above 600 °C, and g-C_3N_4 is completely decomposed at approximately 750 °C. Based on the analysis of the thermal pyrolysis process, the generation of cyano-species around 500 °C is proposed to suppress the sintering of Pt nanoparticles during high-temperature treatment.

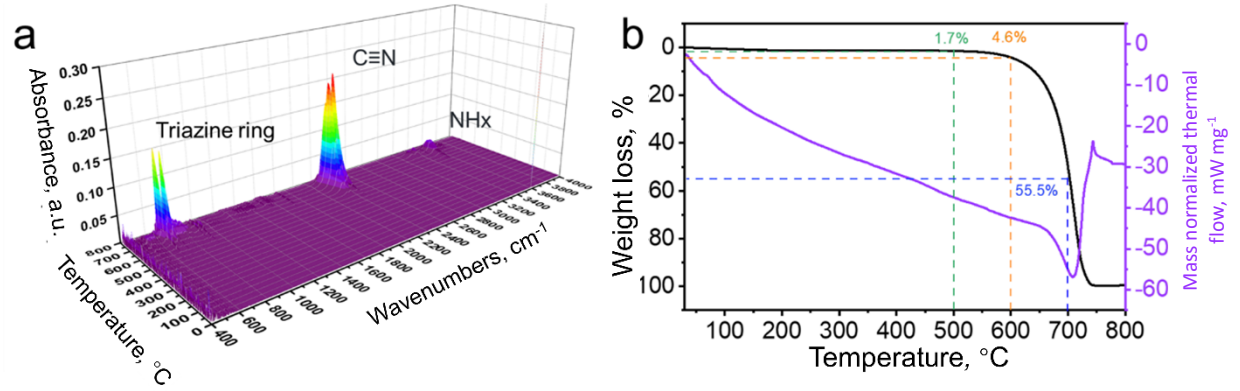

Figure 5. *(a) Thermogravimetry-Fourier transform infrared spectra of evolved gases and (b) thermogravimetry-differential thermal analysis curves of treatment of g-C_3N_4, recorded at 5 °C min^{-1} from 25 to 800 °C*

To further probe the structural evolution of carbon nitride during thermal treatment and its interaction with Pt/C, X-ray photoelectron spectroscopy (XPS) was performed on the carbon nitride-modified Pt/C samples annealed at 500 and 700 °C. At 500 °C, the XPS results reveal clear signatures characteristic of intact g-C_3N_4, as evidenced by the presence of triazine/heptazine-related features in the C 1s and N 1s spectra (Figure 6a and 6b). In contrast, after heat treatment at 700 °C, the contribution from triazine-ring structures in the C 1s region is significantly diminished, indicating substantial decomposition of the carbon nitride framework (Figure 6c). Nevertheless, the N 1s spectra of the 700 °C, treated sample still exhibit discernible components associated with graphitic N and pyridinic N species (Figure 6d). Consistently, the FTIR spectra (Figure 7) show distinct carbon nitride-related vibrational modes at 500 °C, whereas the characteristic triazine-ring vibrations are markedly weakened at 700 °C.

These results collectively suggest that, although the long-range g-C_3N_4 structure is largely decomposed at elevated temperatures, nitrogen-related defects such as graphitic and pyridinic N are retained in the 700°C-treated sample, inherited from the original carbon nitride and potentially contributing to the stabilization of Pt nanoparticles.

XPS wide spectra (Figure 6e) of different samples show that carbon nitride-assisted PtC samples contained C, N, O, and Pt elements. The electronic interaction between Pt and nitrogen species was further examined by Pt 4f X-ray photoelectron spectroscopy (XPS). As shown in Figure 6f, the Pt 4f spectra of the carbon nitride, modified Pt/C, exhibit an apparent shift toward lower binding energies

compared with those of pristine Pt/C. Specifically, the Pt 4f 7/2 peak shifts from approximately 71.2 to 70.9 eV after the introduction of carbon nitride.

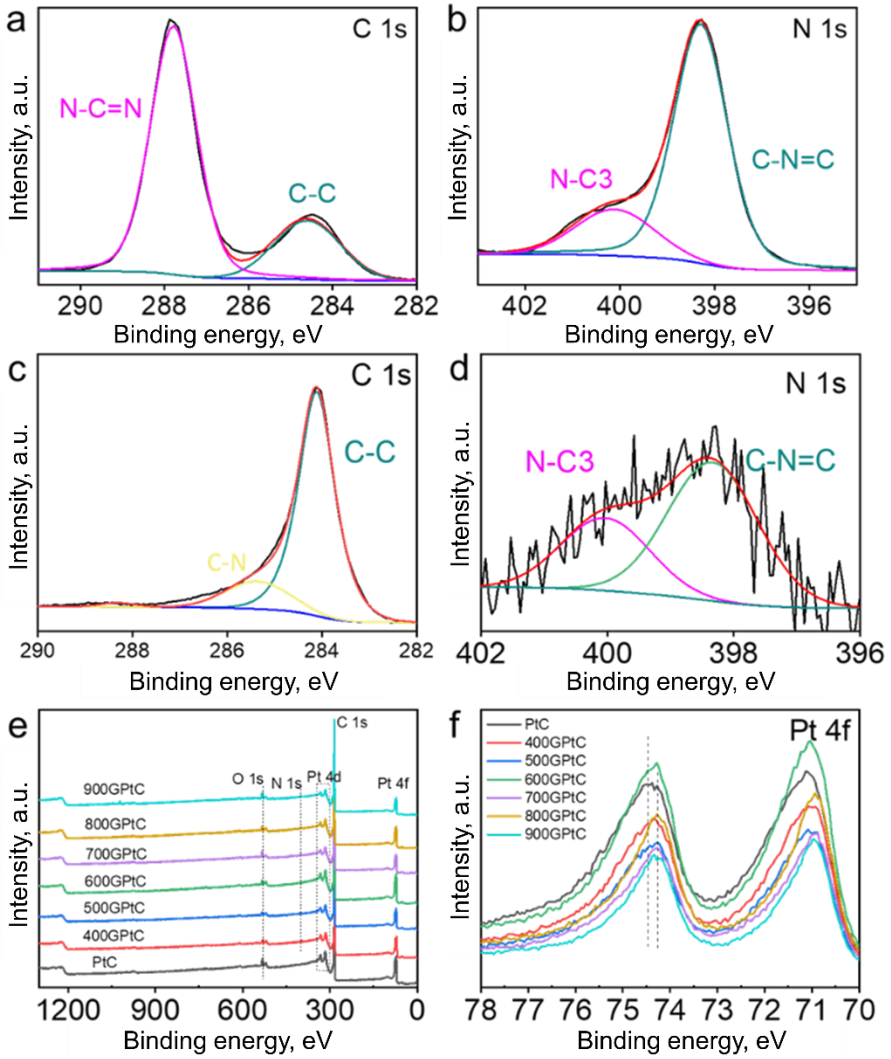

Figure 6. *High resolution C 1 s XPS spectra of (a) 500GPtC and (c) 700GPtC.; high resolution N 1 s XPS spectra of (b) 500GPtC and (d) 700GPtC; (e) XPS wide spectra and (f) Pt 4 f XPS spectra of different samples*

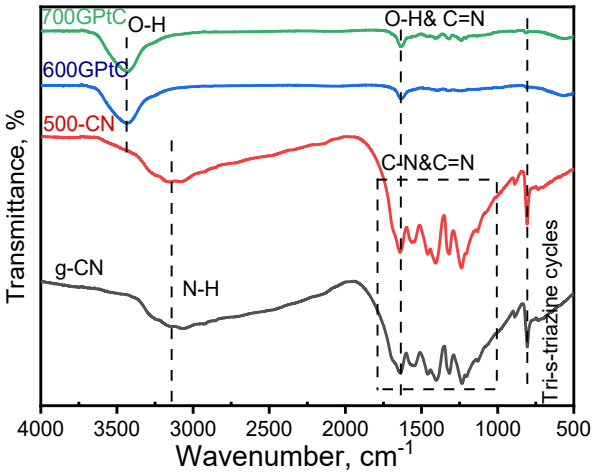

Figure 7. *FTIR spectra of different samples (carbon nitride-assisted Pt/C catalysts were synthesized at 600 and 700 °C, denoted as 600GPtC and 700GPtC, respectively. The sample 500-CN refers to g-C_3N_4 subjected to the same heat treatment at 500 °C, while g-CN denotes pristine g-C_3N_4)*

This negative shift in binding energy suggests an increased electron density on Pt, which is commonly associated with electronic interactions between Pt and nitrogen-containing species. Such electron donation from nitrogen species to Pt is expected to strengthen the metal, support interaction and contribute to the enhanced thermal stability of Pt nanoparticles.

Based on the combined TEM, XRD, TG-FTIR, XPS, and electrochemical analyses, a plausible mechanism for the suppression of Pt nanoparticle sintering by g-C_3N_4 during thermal treatment is proposed. As shown in Figure 8, Pt/C without g-C_3N_4 exhibits significant ripening after heat treatment. During annealing at temperatures around 500 °C, g-C_3N_4 begins to undergo thermal decomposition, accompanied by the generation of nitrogen-containing species, including cyano-related fragments, as evidenced by TG-FTIR analysis.

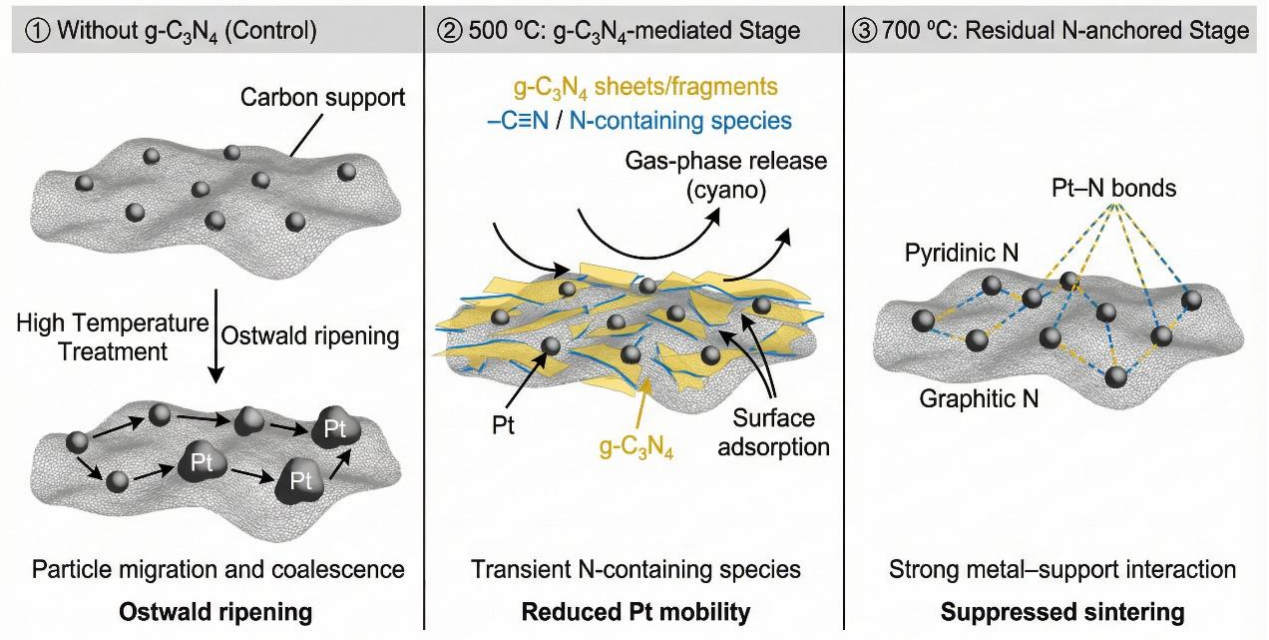

Figure 8. *Schematic illustration of the g-C_3N_4-assisted anti-sintering mechanism of Pt nanoparticles during thermal treatment*

These species, together with the residual carbon nitride framework, are expected to interact with Pt nanoparticles and the carbon support, forming transient or persistent nitrogen-containing surface environments. Such interactions can effectively anchor Pt nanoparticles, reduce their surface mobility, and hinder thermally driven particle migration and coalescence. At elevated temperatures (≥700 °C), although the long-range g-C_3N_4 structure is largely decomposed, XPS and FTIR results indicate the retention of nitrogen-related defects, such as graphitic and pyridinic N species, on the carbon support. These nitrogen functionalities can serve as strong anchoring sites for Pt nanoparticles through electronic interactions, as reflected by the negative shift in Pt 4f binding energy. The enhanced metal-support interaction increases the energetic barrier for Pt atom detachment and surface diffusion, thereby mitigating Ostwald ripening and suppressing particle growth. As a result of these synergistic effects, including transient nitrogen-containing species during intermediate-temperature annealing and stable nitrogen defects at higher temperatures, the g-C_3N_4-assisted Pt/C catalyst exhibits significantly improved resistance to thermal sintering, preserving both nanoparticle size and ORR activity after high-temperature treatment.

The oxygen reduction reaction performance of the catalysts was evaluated by CV and LSV (Figure 9).

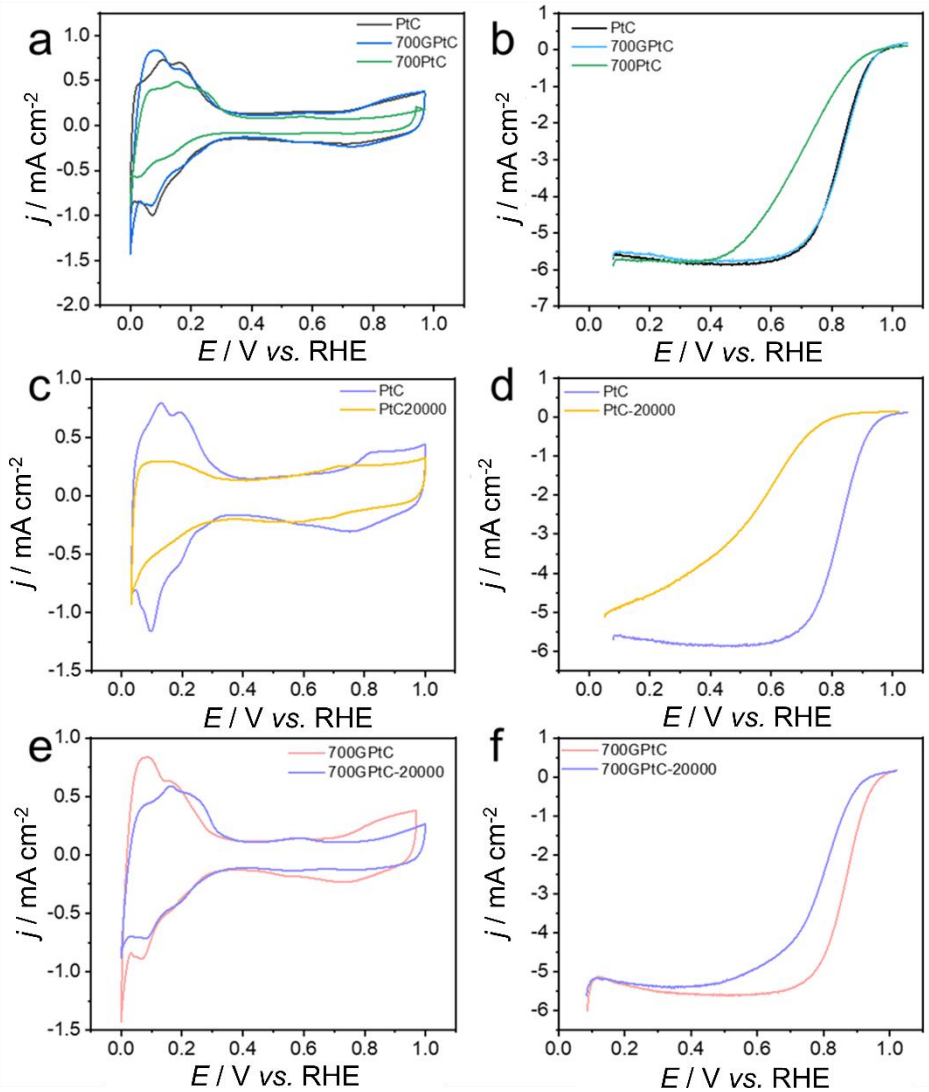

Figure 9. *CV and LSV curves of different Pt/C samples and corresponding accelerated durability testing involving 20,000 potential cycles in 0.1 M $HClO_4$ solution. The sample 700PtC and 700GPtC refer to Pt/C catalysts and the carbon nitride-assisted Pt/C catalysts subjected to heat treatment at 700 °C, respectively. 20000 refers to the measurement taken after 20,000 potential cycles*

After thermal treatment at 700 °C, the carbon nitride-assisted Pt/C catalyst exhibits ORR activity comparable to that of the commercial Pt/C, as reflected by a similar electrochemically active surface area (ECSA) of 69.6 $m^2\ g^{-1}$ (*vs.* Pt/C 69.4) and a half-wave potential of 0.83 V *vs.* RHE. This preserved activity indicates that the addition of carbon nitride effectively suppresses the thermal sintering and ripening of Pt nanoparticles during high-temperature treatment. In contrast, the Pt/C catalyst without carbon nitride shows a pronounced degradation in ORR performance after annealing at 700 °C, characterized by a reduced ECSA of 48.3 $m^2\ g^{-1}$ and a negatively shifted half-wave potential of 0.70 V *vs.* RHE, consistent with severe particle coarsening.

Furthermore, accelerated durability tests revealed that after 20,000 potential cycles, the ORR activity of Pt/C decreases significantly, with the half-wave potential shifting by 331 mV and the ECSA retention dropping to 27.0 %. By comparison, the carbon nitride-assisted, thermally treated Pt/C catalyst exhibits substantially improved durability, showing a much smaller loss in half-wave potential of 72 mV and an ECSA retention of 80.6 % after the same cycling protocol. These results demonstrate that carbon nitride – assisted thermal treatment effectively enhances both the high-temperature stability and long-term ORR durability of Pt/C catalysts.

Conclusions

This work demonstrates that carbon nitride can act as an effective transient stabilizing additive during high-temperature thermal treatment, suppressing Pt nanoparticle sintering on carbon supports. Although the carbon nitride framework partially decomposes at elevated temperatures, the residual nitrogen species remain electronically coupled with Pt, mitigating particle coarsening and preserving catalytic activity. As a result, the carbon nitride-assisted Pt/C catalyst retains ORR performance comparable to commercial Pt/C even after annealing at 700 °C, while exhibiting significantly improved durability during long-term cycling. This strategy provides a simple, scalable, and material-agnostic approach for enhancing the thermal robustness and operational stability of Pt-based electrocatalysts, offering a broadly applicable pathway for the rational design of durable catalysts for fuel cell and related electrochemical energy conversion systems.

Acknowledgment: *This work was financially supported by the Shandong Provincial Natural Science Foundation (No. ZR2022QE109), Qilu University of Technology (Shandong Academy of Sciences) and the Talent Research Project (2023RCKY209).*

Conflict of interest: *There are no conflicts of interest to declare.*

Declaration of generative AI and AI-assisted technologies in the writing process: *The ChatGPT was used to improve the grammar and coherence of the sentence in this manuscript, without affecting the accuracy of the original manuscript. After using this tool, the authors reviewed the whole manuscript and take full responsibility for the content of the published article.*

References

[1] N. Seselj, S. M. Alfaro, E. Bompolaki, L. N. Cleemann, L. T. Torres, K. Azizi, Catalyst Development for High-Temperature Polymer Electrolyte Membrane Fuel Cell (HT-PEMFC) Applications, *Advanced Materials* **35** (2023) 2302207. https://doi.org/10.1002/adma.202302207

[2] X. Ren, Y. Wang, A. Liu, Z. Zhang, Q. Lv, B. Liu, Current progress and performance improvement of Pt/C catalysts for fuel cells, *Journal of Materials Chemistry A* **8** (2020) 24284-24306. https://doi.org/10.1039/D0TA08312G

[3] Z. A. C. Ramli, J. Pasupuleti, N. F. H. N. Zaiman, T. S. T. Saharuddin, S. Samidin, W. N. R. W. Isahak, A. G. N. Sofiah, S. K. Kamarudin, S. K. Tiong, Evaluating electrocatalytic activities of Pt, Pd, Au and Ag-based catalyst on PEMFC performance: A review, *International Journal of Hydrogen Energy* **104** (2025) 463-486. https://doi.org/10.1016/j.ijhydene.2024.04.177

[4] I. E. L. Stephens, A. S. Bondarenko, U. Grønbjerg, J. Rossmeisl, I. Chorkendorff, Understanding the electrocatalysis of oxygen reduction on platinum and its alloys, *Energy & Environmental Science* **5** (2012) 6744-6762. https://doi.org/10.1039/C2EE03590A

[5] W. Chen, Q. Xin, G. Sun, Q. Wang, Q. Mao, H. Su, The effect of carbon support treatment on the stability of Pt/C electrocatalysts, *Journal of Power Sources* **180** (2008) 199-204. https://doi.org/10.1016/j.jpowsour.2008.02.005

[6] L. Gong, J. Liu, Y. Li, X. Wang, E. Luo, Z. Jin, J. Ge, C. Liu, W. Xing, An ultralow-loading platinum alloy efficient ORR electrocatalyst based on the surface-contracted hollow structure, *Chemical Engineering Journal* **428** (2022) 131569. https://doi.org/10.1016/j.cej.2021.131569

[7] S. He, Y. Liu, H. Zhan, L. Guan, Direct Thermal Annealing Synthesis of Ordered Pt Alloy Nanoparticles Coated with a Thin N-Doped Carbon Shell for the Oxygen Reduction Reaction, *ACS Catalysis* **11** (2021) 9355-9365. https://doi.org/10.1021/acscatal.1c02434

[8] V. R. Stamenkovic, B. Fowler, B. S. Mun, G. Wang, P. N. Ross, C. A. Lucas, N. M. Marković, Improved Oxygen Reduction Activity on $Pt_3Ni(111)$ via Increased Surface Site Availability, *Science* **315** (2007) 493-497. https://doi.org/doi:10.1126/science.1135941

[9] Z. Li, J. Zou, X. Xi, P. Fan, Y. Zhang, Y. Peng, D. Banham, D. Yang, A. Dong, Native Ligand Carbonization Renders Common Platinum Nanoparticles Highly Durable for Electrocatalytic Oxygen Reduction: Annealing Temperature Matters, *Advanced Materials* **34** (2022) 2202743. https://doi.org/10.1002/adma.202202743

[10] [D. Wang, H. L. Xin, R. Hovden, H. Wang, Y. Yu, D. A. Muller, F. J. DiSalvo, H. D. Abruña, Structurally ordered intermetallic platinum–cobalt core–sell nanoparticles with enhanced activity and stability as oxygen reduction electrocatalysts, *Nature Materials* **12** (2013) 81-87. https://doi.org/10.1038/nmat3458

[11] S. Chen, Y. Xu, X. Chang, Y. Pan, G. Sun, X. Wang, D. Fu, C. Pei, Z.-J. Zhao, D. Su, J. Gong, Defective TiO_x overlayers catalyze propane dehydrogenation promoted by base metals, *Science* **385** (2024) 295-300. https://doi.org/doi:10.1126/science.adp7379

[12] H. O. Otor, J. B. Steiner, C. García-Sancho, A. C. Alba-Rubio, Encapsulation Methods for Control of Catalyst Deactivation: A Review, *ACS Catalysis* **10** (2020) 7630-7656. https://doi.org/10.1021/acscatal.0c01569

[13] A. Pavlets, I. Pankov, E. Moguchikh, E. Suprun, E.Gerasimov, V. Guterman, A. Alekseenko, Deciphering nanostructural evolution of PtCu/C–N electrocatalyst via identical location transmission electron microscopy imaging: Gram-scale synthesis and superior activity in oxygen reduction reaction, *Journal of Power Sources* **613** (2024) 234898. https://doi.org/10.1016/j.jpowsour.2024.234898

[14] [A. Alekseenko, A. Pavlets, E. Moguchikh, M. Tolstunov, E. Gribov, S. Belenov, V. Guterman, Platinum-Containing Nanoparticles on N-Doped Carbon Supports as an Advanced Electrocatalyst for the Oxygen Reduction Reaction, *Catalysts* **12** (2022) 414. https://doi.org/10.3390/catal12040414

[15] Y. A. Bayan, E. R. Beskopylny, E. U. Gerasimov, E. E. Aydakov, K. K. Volik, I. V. Pankov, I. V. Chepkasov, M. M. Lukanov, A. G. Kvashnin, A. A. Alekseenko, Boosting the Performance of Pt/C Catalysts via Nitrogen-Doped Carbon Support: Insights from Structural and Electrochemical Characterization, *Small* **21** (2025) e10144. https://doi.org/10.1002/smll.202510144

[16] [E. A. Moguchikh, K. O. Paperzh, A. A. Alekseenko, E. N. Gribov, N. Yu. Tabachkova, N. V. Maltseva, A. G. Tkachev, E. A. Neskoromnaya, A. V. Melezhik, V. V. Butova, O. I. Safronenko, V. E. Guterman, Platinum nanoparticles supported on nitrogen-doped carbons as electrocatalysts for oxygen reduction reaction, *Journal of Applied Electrochemistry* **52** (2021) 231-246. https://doi.org/10.1007/s10800-021-01629-y

[17] X.-H. Li, M. Antonietti, Metal nanoparticles at mesoporous N-doped carbons and carbon nitrides: functional Mott–Schottky heterojunctions for catalysis, *Chemical Society Reviews* **42** (2013) 6593-6604. https://doi.org/10.1039/C3CS60067J

[18] L. Wang, C. Wang, X. Hu, H. Xue, H. Pang, Metal/Graphitic Carbon Nitride Composites: Synthesis, Structures, and Applications, *Chemistry-An Asian Journal* **11** (2016) 3305-3328. https://doi.org/10.1002/asia.201601178

[19] I. F. Teixeira, E. C. M. Barbosa, S. C. E. Tsang, P. H. C. Camargo, Carbon nitrides and metal nanoparticles: from controlled synthesis to design principles for improved photocatalysis, *Chemical Society Reviews* **47** (2018) 7783-7817. https://doi.org/10.1039/C8CS00479J

[20] L. Zhang, F. Mao, L. R. Zheng, H. F. Wang, X. H. Yang, H. G. Yang, Tuning Metal Catalyst with Metal–C_3N_4 Interaction for Efficient CO_2 Electroreduction, *ACS Catalysis* **8** (2018) 11035-11041. https://doi.org/10.1021/acscatal.8b03789

[21] M. Najafi, S. Abednatanzi, A. Yousefi, M. Ghaedi, Photocatalytic Activity of Supported Metal Nanoparticles and Single Atoms, *Chemistry -A European Journal* **27** (2021) 17999-18014. https://doi.org/10.1002/chem.202102877

[22] S. Hu, Y. Lei, X. Zhang, F. Zhang, P. Qiao, J. Ye, D. Wang, Recent Advances in Carbon Nitride Supported Single-Atom Catalysts: Synthesis, Characterization, and Applications for CO_2 Photoreduction, *ChemCatChem* **16** (2024) e202301684. https://doi.org/10.1002/cctc.202301684

[23] Y. Wang, X. Wang, M. Antonietti, Polymeric Graphitic Carbon Nitride as a Heterogeneous Organocatalyst: From Photochemistry to Multipurpose Catalysis to Sustainable Chemistry, *Angewandte Chemie International Edition* **51** (2012) 68-89. https://doi.org/10.1002/anie.201101182

[24] S. Cao, J. Low, J. Yu, M. Jaroniec, Polymeric Photocatalysts Based on Graphitic Carbon Nitride, *Advanced Materials* **27** (2015) 2150-2176. https://doi.org/10.1002/adma.201500033

[25] L. Tian, J. Li, F. Liang, S. Chang, H. Zhang, M. Zhang, S. Zhang, Facile molten salt synthesis of atomically thin boron nitride nanosheets and their co-catalytic effect on the performance of carbon nitride photocatalyst, *Journal of Colloid and Interface Science* **536** (2019) 664-672. https://doi.org/10.1016/j.jcis.2018.10.098

[26] J. Li, X. Wang, L. Huang, L. Tian, M. Shalom, C. Xiong, H. Zhang, Q. Jia, S. Zhang, F. Liang, Ultrathin mesoporous graphitic carbon nitride nanosheets with functional cyano group decoration and nitrogen-vacancy defects for an efficient selective CO_2 photoreduction, *Nanoscale* **13** (2021) 12634-12641. https://doi.org/10.1039/D1NR02639A

[27] A. Garcia-Baldovi, M. C. Antonino, L. Peng, L.Tian, S. Goberna-Ferrón, G. Sastre, H. Garcia, M. Antonietti, A. Primo, Synergistic Effect on the Photocatalytic CO_2 Hydrogenation to Methanol Using Dual Co-Cu Single Atom Poly(heptazine imide): Influence of Pressure on Product Selectivity, *ACS Catalysis* **15** (2025) 9584-9596. https://doi.org/10.1021/acscatal.5c00827

[28] L. Tian, J. Li, F. Liang, J. Wang, S. Li, H. Zhang, S. Zhang, Molten salt synthesis of tetragonal carbon nitride hollow tubes and their application for removal of pollutants from wastewater, *Applied Catalysis B: Environmental* **225** (2018) 307-313. https://doi.org/10.1016/j.apcatb.2017.11.082

[29] Y. Jiao, L. Tian, P. García-Aznar, G. Sastre, Y. Li, J. Wang, Z. He, Z. Li, H. García, Enhancement of intramolecular charge transfer in carbon nitride by attaching 2,4,5-Trichlorophenoxyacetic acid as electron acceptor units, *Chemical Engineering Journal* **473** (2023) 145248. https://doi.org/10.1016/j.cej.2023.145248